

Hydra: A mixture modeling framework for subtyping pediatric cancer cohorts using multimodal gene expression signatures

Jacob Pfeil^{1,2*}, Lauren M. Sanders^{1,2,3}, Ioannis Anastopoulos^{1,2}, A. Geoffrey Lyle^{2,3}, Alana S. Weinstein^{1,2}, Yuanqing Xue^{1,2}, Andrew Blair^{1,2}, Holly C. Beale^{2,3}, Alex Lee⁴, Stanley G. Leung⁴, Phuong T. Dinh⁴, Avanthi Tayi Shah⁴, Marcus R. Breese⁴, W. Patrick Devine⁵, Isabel Bjork², Sofie R. Salama^{1,2,6†}, E. Alejandro Sweet-Cordero^{4†}, David Haussler^{1,2,6†}, Olena Morozova Vaske^{2,3†}

1 Department of Biomolecular Engineering, University of California, Santa Cruz, California, United States of America

2 Genomics Institute, University of California, Santa Cruz, California, United States of America

3 Department of Molecular, Cell and Developmental Biology, University of California, Santa Cruz, California, United States of America

4 Department of Pediatrics, Division of Hematology and Oncology, University of California, San Francisco, California, United States of America

5 Department of Anatomic Pathology, University of California, San Francisco, California, United States of America

6 Howard Hughes Medical Institute, University of California, Santa Cruz, California, United States of America

†Senior authorship

* Corresponding author: jpfeil@ucsc.edu

Abstract

Precision oncology has primarily relied on coding mutations as biomarkers of response to therapies. While transcriptome analysis can provide valuable information, incorporation into workflows has been difficult. For example, the relative rather than absolute gene expression level needs to be considered, requiring differential expression analysis across samples. However, expression programs related to the cell-of-origin and tumor microenvironment effects confound the search for cancer-specific expression changes. To address these challenges, we developed an unsupervised clustering approach for discovering differential pathway expression within cancer cohorts using gene expression measurements. The hydra approach uses a Dirichlet process mixture model to automatically detect multimodally distributed genes and expression signatures without the need for matched normal tissue. We demonstrate that the hydra approach is more sensitive than widely-used gene set enrichment approaches for detecting multimodal expression signatures. Application of the hydra analysis framework to small blue round cell tumors (including rhabdomyosarcoma, synovial sarcoma, neuroblastoma, Ewing sarcoma, and osteosarcoma) identified expression signatures associated with changes in the tumor microenvironment. The hydra approach also identified an association between *ATRX* deletions and elevated immune marker expression in high-risk neuroblastoma. Notably, hydra analysis of all small blue round cell tumors revealed similar subtypes, characterized by changes to infiltrating immune and stromal expression signatures.

Author summary

Pediatric cancers generally have few somatic mutations. To increase the number of actionable treatment leads, precision pediatric oncology initiatives also analyze tumor gene expression patterns. However, currently available approaches for gene expression data analysis in the clinical setting often use arbitrary thresholds for assessing overexpression and assume gene expression is normally distributed. These methods also rely on reference distributions of related cancer types or normal samples for assessing expression distributions. Often adequate normal samples are not available, and comparing matched cancer cohorts without accounting for subtype expression overestimates the uncertainty in the analysis. We developed a computational framework to automatically detect multimodal expression distributions within well-defined disease populations. Our analysis of small blue round cell tumors (including rhabdomyosarcoma, synovial sarcoma, neuroblastoma, Ewing sarcoma and osteosarcoma) discovered a significant number of multimodally expressed genes. Multimodally expressed genes were associated with proliferative signaling, extracellular matrix organization, and immune signaling pathways across cancer types. Expression signatures correlated with differences in patient outcomes for *MYCN* non-amplified neuroblastoma, osteosarcoma, and synovial sarcoma. The low mutation rate in pediatric cancers has led some to suggest that pediatric cancers are less immunogenic. However, our analysis suggests that immune infiltration can be identified across small blue round cell tumors. Thus, further research into modulating immune cells for patient benefit may be warranted.

Introduction

Large cancer sequencing projects, including The Cancer Genome Atlas (TCGA) and Therapeutically Applicable Research to Generate Effective Treatments (TARGET), have facilitated the development of cancer gene expression compendia [1–6], but these compendia often lack expression data from corresponding normal tissue. Without the normal comparator, Hoadley et al. (2018) found that cell-of-origin signals drive integrative clustering of TCGA data. Strong cell-of-origin and tumor microenvironment (TME) signals may also complicate the interpretation of gene expression results for precision oncology applications, so careful modeling of the data is necessary to infer accurate conclusions.

The TME includes tumor cells, stromal fibroblasts, immune cells, and vasculature [7]. Similarities in TME composition across tumor samples have led to the identification of TME states (e.g. inflamed, immune-excluded, immune-desert). While these states are dynamic, they can still shed light on the immunogenicity of tumor cells and correlate with response to cancer immunotherapies [8]. The TME cellular composition can be inferred from tumor RNA-Seq data since host cell RNA is sequenced along with the cancer cell RNA. Tumor progression and response to therapies is associated with features of the TME. Therefore, targeting the TME therapeutically may improve treatment outcomes in some cancers.

Immunotherapies that activate the host immune system to eradicate tumors have been effective in treating several cancer types, particularly cancers with a high mutation burden [9, 10]. Pediatric cancers tend to have fewer mutations than adult cancers, and while there has been limited testing of immunotherapies in pediatric cancer patients, the currently available data suggest lower response rates than adult cancers [11, 12]. However, improved immune subtyping of pediatric cancers may identify subsets of patients that are candidates for powerful immunotherapies. In addition to infiltrating immune cells, cancer-associated fibroblasts (CAFs) assist in extracellular matrix remodeling and activation of growth factor signaling. CAFs facilitate tumor growth,

metastasis, and resistance to some therapies, so identification of CAF functions within a tumor may also facilitate clinical decision making. Methods are needed to both infer and characterize gene expression subtypes that correlate with tumor microenvironment states to accelerate the development of personalized therapies for pediatric cancers.

Tumor/normal differential expression analysis in which a cohort of tumor tissues is compared to corresponding normal tissue samples is an effective approach for identifying gene expression biomarkers [13–15], but it is often not possible to conduct this analysis in a clinical setting. Sufficient biological and technical replicates are limited by tumor tissue availability, and healthy neighboring tissue often cannot be isolated. In addition, for many pediatric cancers, the cell-of-origin, and thus the appropriate reference normal tissue, is not known. Besides differential expression analysis, single-sample pathway analysis can be used to identify upregulation of biological gene sets in tumor subtypes. Among the most widely used pathway analysis approaches is gene set enrichment analysis (GSEA) [16, 17]. GSEA identifies coordinated expression of pathway genes using gene ranks and a Kolmogorov-Smirnov-like test statistic. GSEA is usually performed on differentially expressed genes to compare two cohorts or phenotypes, but single-sample GSEA is also available when there is not an obvious comparator. GSEA uses curated pathway gene sets like those in the Molecular Signatures Database (MSigDB) [18].

Cancer gene expression subtypes are traditionally identified using unsupervised clustering methods such as consensus clustering analysis [19–21]. These methods are generally underpowered because the number of genes greatly exceeds the number of samples. Dimensionality reduction approaches such as Principal Component Analysis (PCA) have been found to underestimate the dimensionality of gene expression data [22]. Lenz et al. (2016) found two cases in which PCA fails to identify a biological signal: when the size of the cluster is small and when the effect size is small. Lenz et al. (2016) suggests investigating multimodally expressed genes to improve identification of cancer subtypes. Cancer subtypes naturally lead to multimodal expression patterns because each subtype expresses a correlated set of genes at different expression levels. Expression subtypes may result from dysregulated pathway expression within cancer cells, but another source of multimodal expression comes from varying amounts of infiltrating immune and stromal cells in the TME.

Gaussian mixture models are a powerful class of unsupervised clustering algorithms that can be used to detect multimodally expressed genes [23–25]. A Gaussian mixture model is appropriate when the expression data can be modeled as a mixture of two or more Gaussian distributions [26]. One limitation of Gaussian mixture models in this context is that the number of clusters in the data is often not known beforehand, so a parameter search must be used to identify the best-performing model. However, this is a computationally expensive approach. This problem can be overcome by placing a Dirichlet process prior on the number of expression clusters. The number of clusters is then inferred while fitting the mixture model using Markov chain Monte Carlo (MCMC) sampling [26]. This approach has not been widely used in clinical cancer research because these algorithms are still computationally expensive, but recent advances in Bayesian variational inference have made this approach scalable for precision oncology applications [27].

Here, we present the hydra framework for identifying clinically relevant expression subtypes and classifying N-of-1 tumor samples using learned models. We provide an overview of the hydra framework, assess performance for detecting differential pathway expression, and apply the framework to better understand expression patterns in high-risk neuroblastoma and other small blue round cell tumors. We apply the learned models trained on publicly available cancer gene expression data to the N-of-1 setting and show that this framework can identify distinct immune and stromal expression

signatures that differentiate pediatric cancer samples. Finally, we identify recurrent tumor microenvironment signatures across pediatric cancer types associated with differences in patient outcomes.

Materials and methods

Dirichlet process gaussian mixture model

Traditional parametric models, like the finite mixture model, use a fixed number of parameters (i.e. number of clusters). Over- or underfitting can occur when the parametric model does not reflect the underlying data [28]. Unlike the finite mixture model, the Dirichlet process mixture model (DPMM) represents a theoretically infinite number of clusters and can adapt the number of clusters based on prior belief and the data [26, 28, 29].

The Dirichlet process (*DP*) is an infinite dimensional extension of the Dirichlet distribution [30] and is commonly used as a prior distribution for infinite mixture models [31, 32]. The Dirichlet process has two parameters: the concentration parameter α and centering distribution H . The concentration parameter α , where $\alpha \in \mathbb{R}^+$, controls the extent to which samples from the *DP* resemble the centering distribution H . We model gene expression as a multivariate Gaussian distribution, so our centering distribution is a normal-Wishart distribution ($\mathcal{N}\mathcal{W}_0$).

We briefly describe the stick-breaking construction of the Dirichlet process $G \sim DP(\alpha, H)$. Consider a stick of unit length. To generate an infinite number of mixing weights $\pi_1, \pi_2, \dots, \pi_k$ for the DPMM, first break a stick of unit length at $\nu \in [0, 1]$ where ν is sampled from a Beta distribution, and set π_1 to be the length of the first piece. We repeat this process using the remainder of the stick for each π_k . The DP is truncated to the number of clusters K , which was shown to accurately approximate the infinite posterior for large K [26, 28, 30, 33–35].

$$\nu \sim \text{Beta}(1, \alpha) \quad (1)$$

$$\pi_k = \nu_k \prod_{l=1}^{k-1} (1 - \nu_l) \quad (2)$$

Next, we sample the parameters from the centering distribution H weighted by the mixing components. If we consider a probability space Θ where $\theta_k^* \in \Theta$, then H is a measure on the partitions of Θ . For our application, we will partition the parameter space Θ into finite, measurable partitions B_1, B_2, \dots, B_k .

$$\theta_k^* \sim H \quad (3)$$

$$G = \sum_{k=1}^{\infty} \pi_k \delta_{\theta_k^*} \quad (4)$$

$$(G(B_1), G(B_2), \dots, G(B_k)) \sim \text{Dir}(\alpha H(B_1), \alpha H(B_2), \dots, \alpha H(B_k)) \quad (5)$$

This construction generates the marginal of the Dirichlet process, which follows a Dirichlet distribution. Samples from the marginal distribution are finite, discrete, and sum to 1 [30]. Next, we outline how the DPMM groups gene expression samples x_i under cluster-specific parameters μ_{z_i} and Σ_{z_i} where $z_i \in 1, 2, \dots, K$ is the cluster index.

$$x_i|\mu_{z_i}, \Sigma_{z_i} \sim \mathcal{N}(\mu_{z_i}, \Sigma_{z_i}) \quad (6)$$

$$z_i|\pi \sim \text{Categorical}(\pi_1, \pi_2, \dots, \pi_k) \quad (7)$$

$$\mu_{z_i}, \Sigma_{z_i}|G \sim G \quad (8)$$

$$G|\alpha, \mathcal{NW}_0 \sim DP(\alpha, \mathcal{NW}_0) \quad (9)$$

To improve our methods ability to scale to larger datasets, we incorporated the bnpy memoized online variational inference algorithm (moVB) [33] into our analysis framework. The moVB algorithm uses variational inference to approximate the posterior distribution and interleaves birth, merge, and delete moves to avoid local optima and remove redundant clusters [36]. We found that the moVB algorithm accurately identified the number of clustering on validation datasets (S1 Fig), whereas standard MCMC sampling procedures tended to overestimate the number of clusters.

Hydra method

We developed a Bayesian non-parametric clustering framework for identifying biological and technical variation in large cancer gene expression datasets without the need for a reference normal dataset. To our knowledge, this is the first reproducible and widely deployable implementation of a non-parametric mixture model framework designed to overcome the challenges of precision oncology gene expression analysis. The hydra pipeline is an open source software tool hosted on GitHub (www.github.com/jpfeil/hydra). A Docker container is available for deployment across environments (<https://hub.docker.com/r/jpfeil/hydra>).

The hydra framework contains three main command-line tools: *filter*, *enrich*, and *sweep* (Fig 1). The *filter* command is run first to isolate the multimodally expressed genes using a univariate Dirichlet Process Gaussian Mixture Model (DP-GMM). There are two methods for analyzing the resulting set of multimodally expressed genes. The *enrich* method, which subsets to the genes found to be significantly enriched in biological pathways, and the *sweep* method, which searches within user-defined gene sets for multimodal expression signatures. The underlying analysis routines can be accessed within the Docker using Jupyter notebooks to facilitate the development of user-defined workflows.

The *filter* command (Fig 1B) takes an expression matrix and filters the genes down to the multimodally expressed genes using the DP-GMM described above. We apply a DP-GMM to each gene, saving the model for genes with two or more expression clusters. This creates a directory of multimodally expressed gene models which can be used to predict differential expression in new samples. This analysis framework is a novel contribution to the precision medicine research community. Our approach has several beneficial properties. For example, training models on curated data sets and applying the models to new samples avoids the use of reference distributions, which overestimate the uncertainty in the analysis by not accounting for subtype expression. Furthermore, this approach identifies the set of most strongly differentially expressed genes within a disease context, which may enrich for potential biomarkers for precision medicine applications. The multimodally expressed genes are also used in downstream clustering analysis.

The *enrich* (Fig 1C) and *sweep* (Fig 1D) routines are two independent analyses to explore multimodal expression in cancer gene expression cohorts. In addition to identifying expression variation within a disease context, we also found that multimodally expressed genes that participate in a biological pathway tend to have correlated expression distributions. This insight facilitates the detection of multimodal

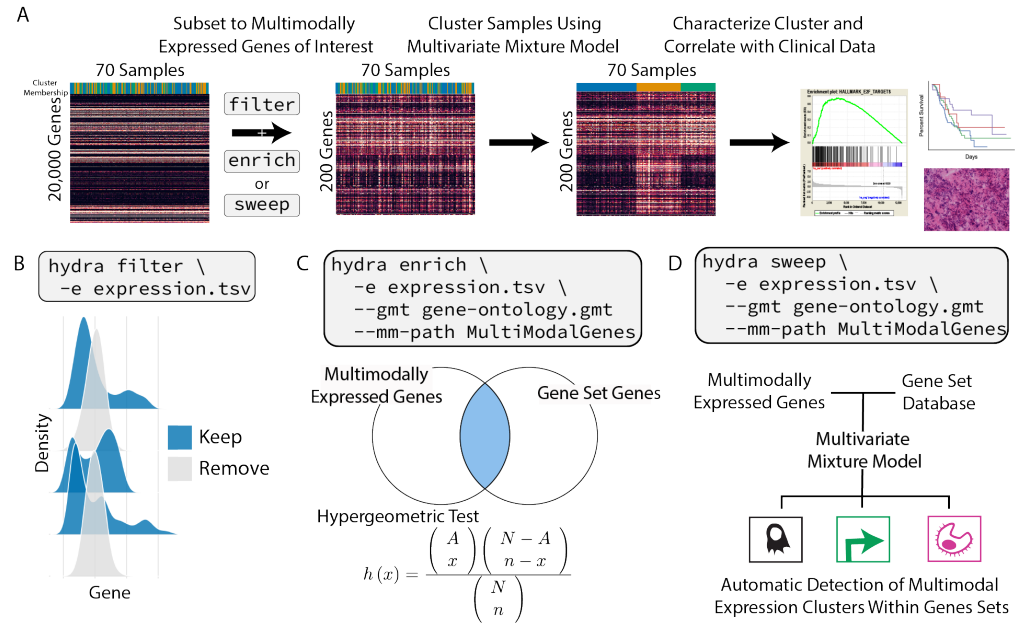


Fig 1. Overview of the hydra framework tools. A: Suggested workflow for applying hydra framework tools to identify clinically relevant gene expression subtypes. B: The hydra *filter* command removes unimodally distributed genes which greatly reduces the number of genes in downstream clustering analysis. C: The hydra *enrich* command takes the multimodally expressed genes and returns enriched gene sets. The enriched gene set genes are used for multivariate clustering of samples. D: The hydra *sweep* command looks for multivariate normal clusters within user-defined gene sets. This can be used for the automatic detection of clusters in large gene set databases.

expression signatures by enriching for genes that have multimodal expression distributions and participate in known biological processes. The hydra software comes prepackaged with popular gene sets, including the Molecular Signatures Database (MSigDB) [18], the Gene Ontology terms [37,38], and the EnrichmentMap gene sets [39]. The gene set database is configurable, so additional gene sets can be added at runtime.

The *enrich* command uses a hypergeometric test [40] to discover enrichment of multimodally expressed genes within a user-defined database of gene sets. This creates a list of gene sets and a list of enriched gene set genes. The *enrich* method outputs a table of enriched gene sets while also clustering samples across the genes that participate in the enriched gene sets. The table of enriched gene sets may reveal surprising expression patterns and generate hypotheses for further investigation of tumor subtypes.

The implementation of the *enrich* method includes an important parameter known as the minimum component probability. The minimum component probability is the probability of placing a sample within the smallest expression cluster. This is an additional filter to remove multimodally expressed genes that influence a relatively small subset of tumor samples. This parameter gives the user the ability to subset the enriched genes to those that influence a greater number of patients. To aid in the exploration of minimum component thresholds, we implemented a *scan* sub-routine. The *scan* routine tunes the analysis with respect to the constraints of the available data (e.g. number of samples and number of genes), which is an important factor in pediatric cancer research since data is often difficult to obtain and so datasets are relatively small. We recommend setting this threshold such that the number of genes is less than the number of samples because otherwise the inference may become unstable [41].

The *sweep* routine identifies differentially expressed gene sets and can be used as an alternative to single-sample GSEA [16]. For each gene set, a multivariate DP-GMM is applied to determine if more than one expression cluster is present within the gene set. This approach is useful when curated gene sets are available for the disease of interest, but manual inspection of each gene set is not feasible. Reducing the genes to multimodally expressed genes facilitates the detection of differentially expressed gene sets. Existing gene set enrichment tools are known to under-perform when the expression is correlated [42], but our approach is designed to identify distinct correlation structures within gene expression datasets.

We have also implemented routines for cluster profiling and N-of-1 tumor analysis. These routines are accessible within the docker container using the Jupyter notebook command. Cluster profiling analysis of clusters derived from the *enrich* or *sweep* routines includes GSEA [43] to identify the pathway expression that characterizes each cluster. GSEA uses all available genes since it requires non-differentially expressed genes to assess the significance of an enrichment score. A t-statistic is calculated for each gene, comparing gene expression values of samples inside to those outside of a cluster. Cluster profiling GSEA uses the ranked gene-level t-statistics to determine gene set enrichment.

The N-of-1 tumor analysis routine classifies a new gene expression profile into one of the inferred clusters, calculates a gene-level z-score for that sample relative to the normalized expression distribution, and performs standard GSEA using a preranked list of z-score values [43]. This procedure can identify new gene expression signatures that may not be detectable using the entire expression cohort as a background reference distribution. This approach is another novel contribution to the field and may facilitate the identification of clinically relevant signatures that are being overlooked in current gene expression analyses.

Synthetic data generation and validation

We first tested the hydra framework's ability to detect differential pathway expression using synthetic cancer data. We compared hydra *sweep* to two widely used gene set enrichment tools: single-sample gene set enrichment analysis (ssGSEA) and gene set variation analysis (GSVA) [44–46]. Both methods are implemented in the GSVA R package [45]. In order to accurately model correlation structures within cancer cohorts, we modeled the synthetic cancer gene expression data as a multivariate Gaussian distribution. We used the TCGA glioblastoma multiforme (GBM) cohort (N=166) to model a background mean and covariance matrix for the synthetic data analysis. We chose TCGA GBM, a very different disease from those analyzed in the remainder of this manuscript, to avoid overfitting the hydra method to diseases of interest. This also enables us to demonstrate the flexibility of our method to analyze data from a variety of cancer genome sequencing projects.

This approach allowed us to model cancer gene expression data while also controlling for subtype-related expression variation. We downloaded the RSEM-quantified TPM normalized gene expression measurements from the UCSC Xena Browser [3]. We focus our analysis on normalized gene expression data because this data is more widely used in the cancer research community and fewer methods are available to analyze normalized counts. To reduce heteroscedasticity and the effect of outlier expression levels, we transformed the expression data to $\log_2(\text{TPM} + 1)$ [47].

We defined an expression subtype as a subset of samples with a distinct expression mean and correlation structure compared to other samples within the disease cohort. To avoid biases in the synthetic data generation process, we used random sampling to select MSigDB gene sets for each subtype, the size of the subtype, and the correlation structure within the subtype. We randomly generated a covariance matrix for the cancer subtype expression data, but used the underlying covariance matrix of the

TCGA glioblastoma multiforme dataset for the background samples. We tested the
231 effect of having 10% and 25% of genes within a gene set being differentially expressed
232 (%DEG). In addition to these parameters, we tested a range of effect sizes: 0.25 (least
233 different), 0.5, 0.75, 1.0, 1.5, 2.0, 2.5, and 3.0 (most different). This process was
234 repeated twice for each gene set to create synthetic training and test data, which
235 resulted in the generation of 640 synthetic datasets.
236

We then applied the hydra framework using the *hydra sweep* command (Fig 1C),
237 since this method is directly comparable to the single-sample GSEA methods. The
238 mean expression filter removed any genes with a mean expression of fewer than $1.0 \log_2(TPM + 1)$.
239 This avoids lowly-expressed genes that may have particularly noisy
240 expression measurements. The prior on the hydra covariance matrix was the identity
241 scaled by 2.0 and the prior on the number of clusters was set to 2 because we expect
242 there to be an activated cluster and a baseline expression cluster. We set the
243 over-expressing cluster to be the cluster with the largest L1 norm.
244

Pediatric cancer gene expression data

We downloaded pediatric cancer RNA-Seq data for neuroblastoma, osteosarcoma,
246 Ewing sarcoma, alveolar rhabdomyosarcoma, and embryonal rhabdomyosarcoma from
247 the UCSC Treehouse Compendium
248 (<https://treehousegenomics.soe.ucsc.edu/public-data/>). This data was
249 produced using the same RNA-seq pipeline, so potential computational batch effects are
250 minimized [1, 6]. Clinical data for the TARGET neuroblastoma and osteosarcoma
251 samples were obtained from the TARGET Data Matrix
252 (<https://ocg.cancer.gov/programs/target/data-matrix>). We also analyzed a set of 58
253 synovial sarcoma microarray profiles with matching metastasis rate data [48].
254

TARGET neuroblastoma analysis

We applied each hydra tool to the TARGET *MYCN-NA* neuroblastoma cohort. We
255 first obtained the multimodal gene models using the *hydra filter* tool. The *hydra filter*
256 tool identified all genes with a multimodal expression pattern. We used the mean
257 expression filter to remove genes that may have unstable measurements due to low
258 transcript abundances. We excluded all genes with a mean expression value less than $1 \log_2(TPM + 1)$.
259

The *hydra sweep* command was applied to search for subtype expression within
260 curated MSigDB gene sets. We included the hallmark (n=50), BioCarta (n=289),
261 KEGG (n=186), PID (n=196), and Reactome (n=1499) genesets [18]. We include all
262 signatures with a minimum component probability of 10%. For example, the smallest
263 subtype cluster considered in this analysis had 7 samples, since the total number of
264 samples was 70. We investigated relationships among differentially expressed gene sets
265 by clustering the gene sets by their pairwise Jaccard index. This created a similarity
266 network that was then visualized using the Gephi software tool [49].
267

The *hydra enrich* command identified correlated expression signatures using the
268 enriched GO term genes ($FDR < 0.01$). The multivariate mixture model α
269 concentration parameter was set to 5.0; the prior on the covariance matrix was set to
270 the identity scaled by 2.0. The prior parameter for the number of clusters was set to 5.
271 Our synthetic data analysis found that the signal decreases below an effect size of 1.0,
272 so we use this parameter value for all following analyses. We used the *hydra scan*
273 routine to search a range of minimum component probability thresholds (see Results)
274 and found that a threshold/probability of 20% yielded the most clusters while keeping
275 the number of genes ($p = 42$) below the number of samples ($n = 70$).
276

To validate tumor microenvironment expression subtypes, we correlated the hydra *enrich* expression clusters with the results of tumor microenvironment profiling tools xCell [50], CIBERSORT [51], and ESTIMATE [52]. We also compared the hydra *enrich* approach to state-of-the-art consensus clustering methods M3C [20] and k-means clustering using the Gap statistic to select the number of clusters [53]. Since these methods are influenced by the number of input genes, we tested a range of median absolute deviation (MAD) thresholds. The number of clusters was assumed to be the smallest statistically significant value.

Small blue round cell tumor analysis

We then compared the clustering patterns across *MYCN*-NA neuroblastoma, osteosarcoma, Ewing sarcoma, embryonal rhabdomyosarcoma, alveolar rhabdomyosarcoma, and synovial sarcoma. We applied the TumorMap dimensionality reduction method [5] to visualize clustering of the full small blue round cell tumor gene expression matrix. We then applied the hydra framework to explore expression variation within each disease. Each disease expression matrix had unique statistical properties including sample size and subtype variation. This required us to adapt the minimum probability threshold for each disease dataset using the *scan* routine. The Jupyter notebooks for exploring these datasets can be found on GitHub (www.github.com/jpfeil/hydra-paper/analysis). We used agglomerative clustering to investigate patterns in the top 10 enriched gene sets for each disease's expression subtypes.

Statistical analysis

A Kruskal-Wallis test was used to identify statistically significant differences across two or more groups, and a Mann-Whitney U test was used for pairwise tests using a Holm-Sidak correction for multiple hypothesis testing [54, 55]. We used the *scipy* [56] stats implementation of the Kruskal-Wallis test and the *scikit-learn* post hoc processing [57] implementation of pairwise Mann-Whitney U tests. Spearman rank and Pearson correlation values were calculated using the *scipy* library [55]. Survival analysis was done using the *survminer* package [58].

H&E slide preparation and pathologist review

Pediatric tumor samples were flash frozen, embedded in OCT, and 5 μ m cryosections were collected. Slides were hematoxylin and eosin (H&E) stained and imaged on a Leica DMi8, equipped with a HC PL APO 40x/0.85 NA objective and DFC7000T camera. H&E slides were reviewed by a licensed pathologist. Morphologic analysis was performed and the degree and type of inflammation estimated from the histologic sections. Grading of inflammation was either minimal (<10% of total nuclei consist of inflammatory cells) or moderate (20-30% of total nuclei consist of inflammatory cells). The type of inflammation (predominantly small mature lymphocytes or mixed inflammation consisting of small mature lymphocytes along with plasma cells and/or eosinophils) was noted for each tumor sample.

Results

Performance assessment using synthetic gene expression data

To assess how well hydra detects differentially expressed pathways as compared to common pathway enrichment approaches, we applied the hydra framework to

synthetically-generated cancer gene expression data. We generated synthetic cancer gene expression data based on the TCGA glioblastoma multiforme and the MSigDB Hallmark gene sets as described above. We tested a range of effect sizes and percent differentially expressed genes (%DEG) within the MSigDB gene sets. We generated receiver operator curves (ROC) and calculated the area under the receiver operator curve (AUC) for each analysis. Overall, the hydra pipeline outperformed the single-sample GSEA approaches with a mean AUC of 0.93 (95% CI: 0.91 - 0.95). ssGSEA had a mean AUC of 0.72 (95% CI: 0.71 - 0.74) and GSVA had a mean AUC of 0.67 (95% CI: 0.66 - 0.68) (Fig 2A).

We further investigated the performance of these methods by plotting the AUC against the effect size at 10 and 25%DEG (Fig 2B). The hydra method performed better across all effect sizes, achieving near perfect performance above an effect size of 2.0 and 0.75 at 10 and 25%DEG, respectively. ssGSEA and GSVA performed similarly at low effect sizes, but ssGSEA performed better than GSVA as the effect size increased. Overall, the hydra framework performed significantly better than these standard gene set enrichment approaches, particularly at low effect sizes. Therefore, the hydra approach is better suited for subtyping within a disease cohort when the effect sizes are smaller and fewer genes are differentially expressed.

We performed a runtime analysis comparing hydra *sweep*, ssGSEA, and GSVA for identifying a single differentially expressed gene set, since these methods are directly comparable. Training the hydra model was the most computationally expensive step, but the classification of new samples was very fast. The average runtime for the hydra *sweep* algorithm was similar to ssGSEA, but the hydra runtimes were more variable across effect-sizes and number of differentially expressed genes. The GSVA approach was faster than hydra *sweep* and ssGSEA, but GSVA performed worse on the synthetic data analysis than ssGSEA and hydra. We repeated the above analysis with an effect size of 1.0, a %DEG of 25%, and a range of sample sizes, including 50, 100, 200, 300, 400, 500, 1000 samples. The hydra *sweep* and GSVA methods scaled well to large sample sizes, but the ssGSEA runtime increased exponentially as the sample size increased (Fig 2C & D).

Hydra analysis of high-risk neuroblastoma

High-risk neuroblastoma is an aggressive disease and is resistant to intensive therapy. Further subtyping of high-risk neuroblastoma may identify novel therapeutic targets and improve risk stratification. We hypothesized that unsupervised clustering of multimodally expressed genes associated with enriched Gene Ontology terms would identify expression subtypes of high-risk neuroblastoma tumors. TumorMap analysis [5] showed that the *MYCN*-non-amplified (*MYCN*-NA) neuroblastoma samples clustered separately from *MYCN*-amplified (*MYCN*-A) and stage 4S neuroblastoma samples (S2 Fig). We focused on the *MYCN*-NA neuroblastoma tumor samples because this is the largest set of samples (N=70) and variation within *MYCN*-NA tumors is not well understood [59].

We applied the hydra *filter* analysis to the TARGET high-risk neuroblastoma cohort as described above. This analysis identified 931 genes within the *MYCN*-NA neuroblastoma cohort with a multimodal expression distribution. Of the 931 multimodally expressed genes, 358 genes were found to be potentially druggable by the Drug Gene Interaction Database (S1 File) and 60 genes were associated with an FDA-approved, anti-neoplastic drug [60].

We next examined whether unsupervised clustering of multimodally expressed genes revealed coordinated expression of annotated gene sets within the MSigDB database. Applying the hydra *sweep* command to the *MYCN*-NA neuroblastoma cohort discovered 105 gene sets with multimodal expression patterns. Each gene set sheds light

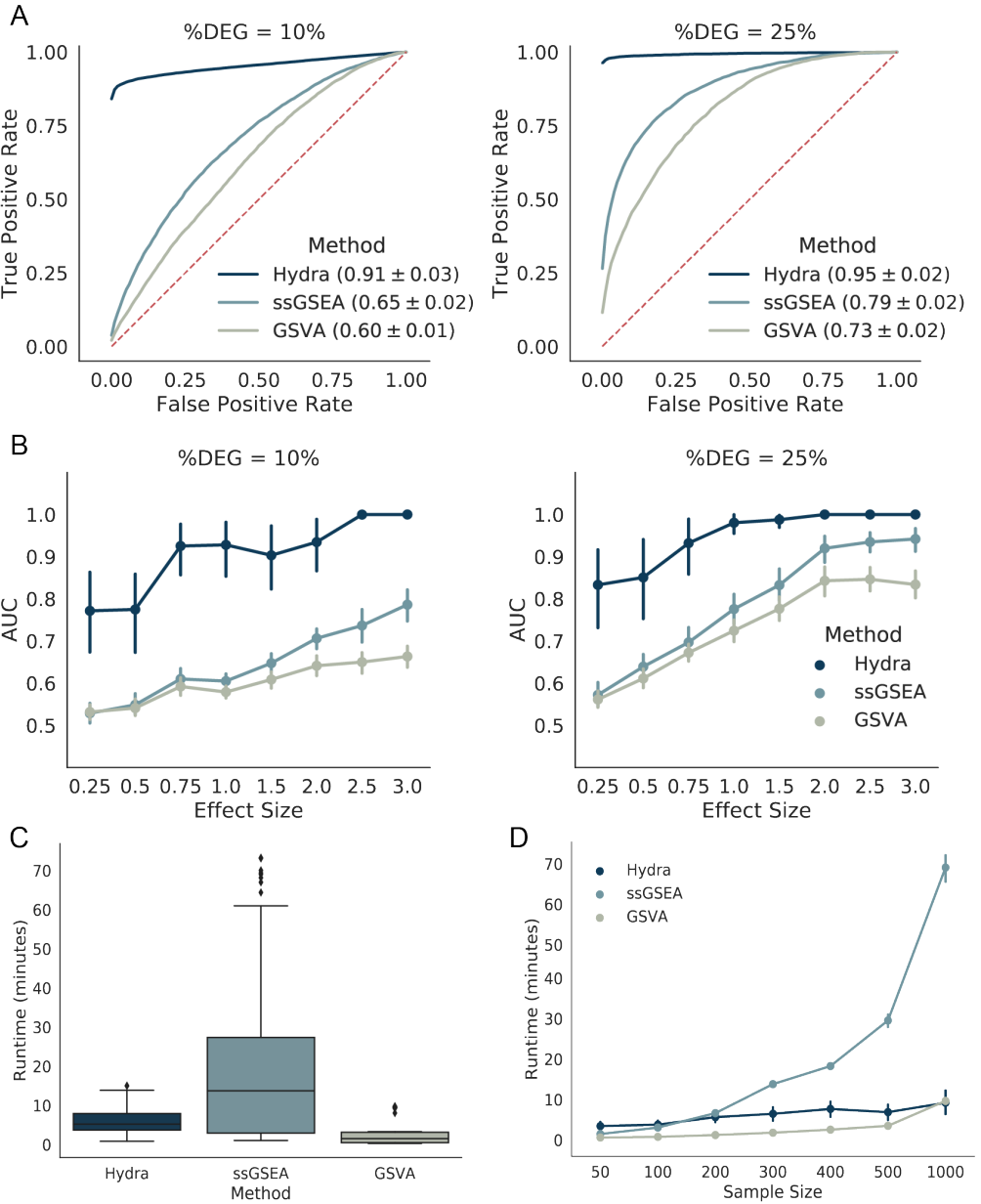


Fig 2. Hydra sweep is more sensitive than existing gene set enrichment approaches for detecting differential pathway expression in synthetic data and scales well to large datasets. A: Mean receiver operator curves across effect sizes, percent differentially expressed genes (%DEG), and MSigDB Hallmark gene sets. A larger area under the curve (AUC) indicates better performance. The average AUC and 95% confidence interval for each method are in the ROC plot figure legends. B: Line plots comparing the mean AUC across a range of effect sizes and %DEG values. C: Box plot showing mean runtimes for differential pathway analysis where the effect size is fixed but the sample size varies. D: Line plot comparing the mean runtimes for differential pathway analysis across a range of sample sizes.

on biological themes that are differentially expressed within the *MYCN-NA* neuroblastoma cohort. We clustered the differentially expressed gene sets to reveal these

biological themes (S4 Fig). We found 6 major themes, including annotated cancer functions, cell cycle regulation, cell signaling pathways, immune functions, extracellular matrix reorganization, and metabolic pathway gene sets.

We applied the hydra *enrich* analysis to the MYCN-NA cohort to identify how the most highly enriched gene sets interact to form expression subtypes. This analysis found 428 genes with a minor component probability greater than 20% (S1 File). Gene Ontology analysis found enrichment for the following GO terms (FDR: $q < 0.01$): adaptive immune response (24 genes), mesenchyme development (12 genes), steroid hormone secretion (4 genes), and response to corticosterone (4 genes). DP-GMM analysis of the 44 enriched GO term genes identified three *MYCN*-NA neuroblastoma clusters (Fig 3A). The posterior probability for belonging to each cluster was 42%, 34%, and 17% for clusters 1, 2, and 3, respectively. The posterior probability for a sample belonging to a new cluster was about 6% in our analysis.

We next investigated cluster-specific expression signatures using GSEA (see Hydra Method section). Cluster 1 was enriched for adaptive immune response gene sets, cluster 2 was enriched for proliferative signaling gene sets, and cluster 3 was enriched for cancer-associated fibroblast gene sets (Fig 3B). Cluster 3 shares several features of a wound healing response, including fibroblast recruitment, extracellular matrix organization, and infiltration of immune cells [61].

Clusters 1 and 3 were enriched for tumor microenvironment-associated gene expression. To further validate this signal, we correlated the hydra clusters with enrichment scores from the tumor microenvironment profiling tools xCell [50] and ESTIMATE [52]. Cluster 1 had high average xCell enrichment scores associated with adaptive immune cell types including B-cells, CD4+ naive T-cells, and CD8+ naive T-cells (Kruskal-Wallis: $p < 0.001$). Cluster 2 was characterized by the absence of immune and stromal expression and higher tumor purity scores than clusters 1 and 3. The average ESTIMATE tumor purity was 88%, 96% and 82% for clusters 1, 2, and 3, respectively. Cluster 3 was enriched for fibroblast-associated expression by xCell analysis (Kruskal-Wallis: $p < 0.001$). Clusters 1 and 3 had higher ESTIMATE immune-associated expression levels than cluster 2 (average ImmuneScore per cluster: 58, -612, 56), but cluster 3 had the highest stromal expression signature score (average StromalScore per cluster: -1027, -1310, -135). Comparing ESTIMATE enrichment scores across clusters reveals clear trends in broad immune and stromal expression signatures. Lastly, we found a correlation between the hydra-identified tumor microenvironment subtype and *CD274* and *CTLA4* expression (S6 Fig)

We next correlated clusters with clinical features. We found no difference in patient survival outcomes across clusters (log-rank test, $p > 0.05$). Notably, cluster 1, which had the highest adaptive immune expression signal in MYCN-NA neuroblastoma, over-expresses cell-cycle regulation genes, which was not observed in other small blue cell tumors. We investigated associations with clinical covariates, including mutation burden, age, and tumor content as assessed by a clinical pathologist, but found no statistically significant differences (Kruskal-Wallis: $p > 0.05$). We then investigated associations between the hydra clusters and neuroblastoma-associated molecular aberrations and clinical features (S1 File). *ATRX* gene deletions were enriched in cluster 1 (Fisher's Exact Test: $p < 0.05$). MKI low tumors were enriched in cluster 2 and 3 (Fisher's Exact Test: $p < 0.01$). Chromosome 17 wild-type tumors were enriched in clusters 2 and 3 (Fisher's Exact Test: $p < 0.01$). Analysis on a larger dataset may reveal additional clusters and correlations with clinical features.

Consensus clustering is a widely used approach for identifying tumor subtypes using gene expression data. We applied the M3C consensus clustering method, which is a more sophisticated version of consensus clustering that uses a null distribution to assess the statistical significance of the clustering [20,21]. We used the top 5000 genes with the

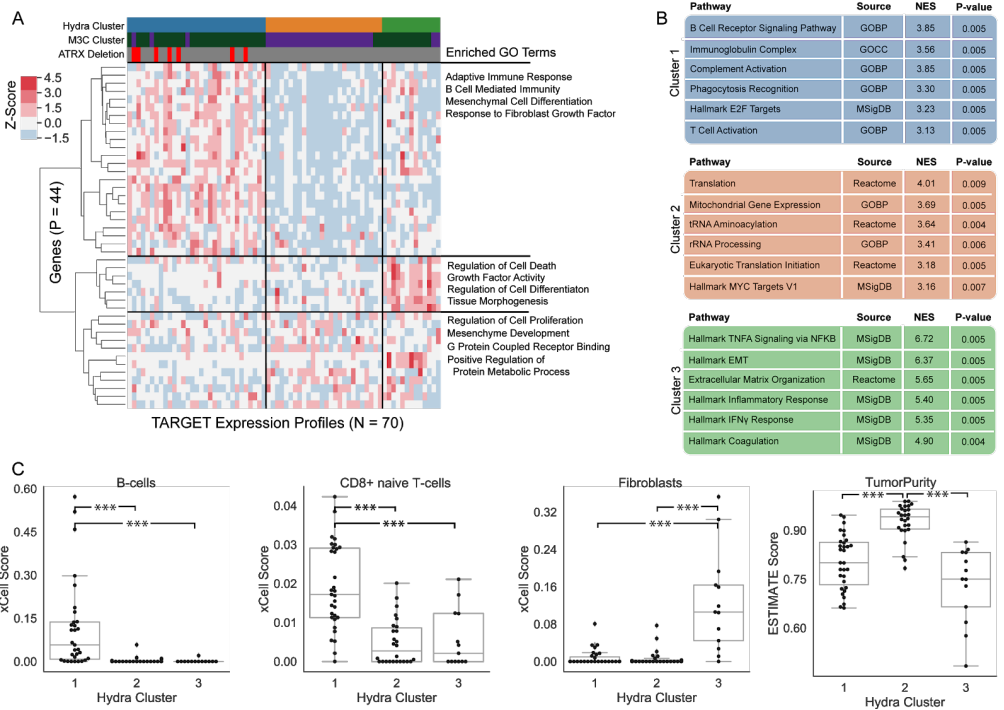


Fig 3. Hydra analysis identifies three distinct tumor microenvironment expression subtypes in *MYCN* non-amplified neuroblastoma samples. A: Gene expression heatmap displaying expression profiles of hydra clusters. Heatmap columns (samples) are ordered by hydra cluster membership. Ward hierarchical clustering applied to rows (genes) identified coordinated expression of GO term genes. These GO term genes were originally identified by the hydra *enrich* command. B: GSEA performed on each cluster identified enrichment of tumor microenvironment and proliferative signaling gene sets. C: xCell enrichment score distributions for B-cells, CD8+ naive T-cells, and Fibroblasts, and the ESTIMATE TumorPurity score distributions for each cluster; enrichments for all cell types are available in S1 File. Abbreviations: Normalized Enrichment Score (NES), Epithelial to Mesenchymal Transition (EMT), Gene Ontology Biological Process (GOBP).

largest median absolute deviation (MAD) because this threshold is routinely used in unsupervised clustering of cancer gene expression data [62–64].

The M3C analysis resulted in the identification of two statistically significant clusters. One M3C cluster correlated with hydra clusters 1 and 3 and the other M3C cluster correlated with hydra cluster 2. Therefore, M3C clustering detected the tumor purity signal in the expression data, but was not able to separate the adaptive immune cell and fibroblast infiltrated clusters (hydra clusters 1 and 3). We also applied k-means clustering using the gap statistic approach [53, 65] for estimating the number of clusters, but this approach grouped all samples into a single cluster. We tested a range of MAD thresholds based on the median absolute deviation, but found similar results across thresholds (S3 Fig). Overall, the hydra approach was more sensitive at detecting distinct tumor microenvironment states than these other popular clustering methods.

To further investigate expression patterns within the hydra-identified tumor microenvironment subtypes, we performed GSEA by z-score normalizing each tumor's gene expression data to its tumor microenvironment cluster. This is a novel GSEA approach that uses the tumor microenvironment state discovered by the hydra method

to identify additional gene expression signals for individual samples. This approach revealed signals not present at the cohort level analysis (Fig 4). For example, enrichment of immune expression signatures within cluster 2 predicted differences in overall survival such that patients with higher immune expression had a better overall survival rate. Similarly, an elevated cell cycle signal within cluster 3 predicted worse survival compared to other cluster 3 samples with lower cell cycle expression. A metastatic expression signal was identified in the analysis of cluster 1 samples, but this signature did not correlate with a difference in survival. This approach may therefore provide appropriate background distributions for revealing and evaluating the significance of gene expression patterns and survival statistics within tumor subtypes.

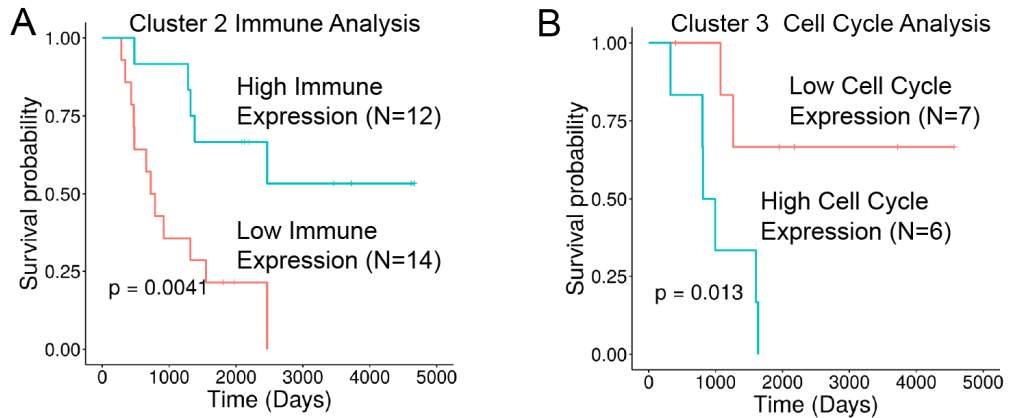


Fig 4. Gene set enrichment analysis (GSEA) of MYCN-NA neuroblastoma identifies overall survival differences within hydra cluster 2 and cluster 3. Cluster-level GSEA separated cluster 2 into high and low immune expression subtypes and cluster 3 into high and low cell cycle expression subtypes. A: Kaplan-Meier plot for immune expression subtypes within cluster 2. B: Kaplan-Meier plot comparing cell cycle expression subtypes within cluster 3.

N-of-1 tumor analysis for pediatric neuroblastoma

The command-line interface of the hydra toolkit includes a *predict* function for labeling samples using a pre-fit model. The *MYCN-NA* neuroblastoma model described above was used to predict expression subtypes on a new set of samples. We obtained tumor gene expression data from six stage 4, *MYCN-NA* neuroblastoma samples from the UCSC Treehouse gene expression compendium [5, 6]. The age at diagnosis ranged from 2 to 6 years. Four out of six samples had a deletion in the *ATRX* gene.

Application of the hydra N-of-1 analysis framework clustered 4 out of the 6 samples into cluster 1, which is characterized by adaptive immune cell expression. Three of the *ATRX*-deleted samples clustered with the high adaptive immune cell expression cluster (cluster 1) and one clustered in the low immune, high proliferative signaling cluster (cluster 2). We showed earlier that tumors with *ATRX* deletions tend to have higher adaptive immune expression, and we found a similar pattern in an independent set of *MYCN-NA* neuroblastoma samples.

Two of the samples with loss of *ATRX* came from the same patient but at different timepoints. The first sample (diagnostic sample) clustered with high adaptive immune cell expression (cluster 1), but the resection sample clustered with the low immune expression, high proliferative signaling cluster (cluster 2). We investigated possible explanations for the change in tumor microenvironment state. We performed GSEA

comparing the samples from different timepoints to investigate potential mechanisms leading to immune evasion in these samples. GSEA found downregulation of the MHC Class I Antigen Processing & Presentation GO term in the resection sample (adjusted p-value < 0.002). Loss of antigen processing functions is a common mechanism of immune evasion across cancer types [66].

We obtained H&E stained sections for each of the hydra-identified clusters (S5 Fig). The cluster 1 sample had moderate levels of inflammation (30-50%) consisting of mature mononuclear cells, plasma cells, and eosinophils. The cluster 2 sample had minimal levels of inflammation (<10%) with some scattered mature mononuclear cells throughout the tumor. The cluster 3 sample looked similar to the cluster 1 slide with moderate levels of inflammation (30-50%), but also had regions of apparent necrosis. The inflammation and necrosis in the cluster 3 sample may correlate with the tissue remodeling/wound healing signature identified in the expression data.

Hydra analysis discovers complex tissue signatures

While the *MYCN*-NA neuroblastoma analysis above focused on immune and wound healing expression signatures, the hydra *enrich* method is unsupervised and can therefore detect any type of expression signature. To illustrate this, we applied the hydra *filter/enrich* analysis to the TARGET osteosarcoma cohort (N=74) and discovered enrichment of the GO striated muscle contraction term (FDR < 0.01, Fig 5). Multivariate clustering for the GO striated muscle contraction gene set using the *sweep* routine identified two clusters. xCell analysis of the osteosarcoma cohort found significant enrichment of skeletal muscle expression in the second cluster (Mann-Whitney U test, p < 0.001). Surprisingly, the M3C clustering approach was not able to detect the strong muscle signature using the 5000 genes with the largest MAD (p > 0.05). We used the muscle expression signature to identify osteosarcoma tumors in the UCSC Treehouse Compendium which also contained a similar expression signature. We subsequently confirmed with a licensed pathologist that one of the muscle-expression positive tumor samples did contain significant muscle tissue infiltration. The hydra *enrich* analysis revealed expression signatures not routinely investigated when analyzing osteosarcoma data. Nevertheless, these signals contribute significantly to the tumor expression profile, so explaining these sources of variation is necessary to derive clinically relevant conclusions from gene expression data.

We applied the *filter* method to Ewing sarcoma and discovered multimodal expression of an important druggable gene, JAK1. Applying the multimodal expression model allowed us to deconstruct the Ewing sarcoma distribution into three components (S7 FigA). We found that the expression component with the highest JAK1 expression was also enriched for mast cell expression (S7 FigB). Therefore, overexpression of JAK1 may not correspond to activation of the JAK/STAT signaling pathway in cancer cells but rather to the presence of mast cells within the tumor microenvironment. Furthermore, targeted inhibition of JAK1 using ruxolitinib was shown to inhibit essential mast cell functions, including degranulation [67]. Therefore, therapeutic intervention intending to inhibit JAK1 expression in cancer cells may inadvertently inhibit the patient's mast cell functions. Overexpression analysis using the Ewing sarcoma JAK1 expression distribution may identify JAK1 as an actionable lead, but further investigation into the effect of inhibiting off-target JAK1 expression in mast cells is needed. The hydra framework facilitates the identification of important expression signatures which can be used to deconstruct complex tumor expression subtypes and identify potentially confounding expression signals.

We next quantified the number of multimodal druggable genes from the *MYCN*-NA neuroblastoma dataset that correlated with at least one xCell cell type signature. Out of the 358 druggable genes, we found that 77 correlated with a non-cancer cell type

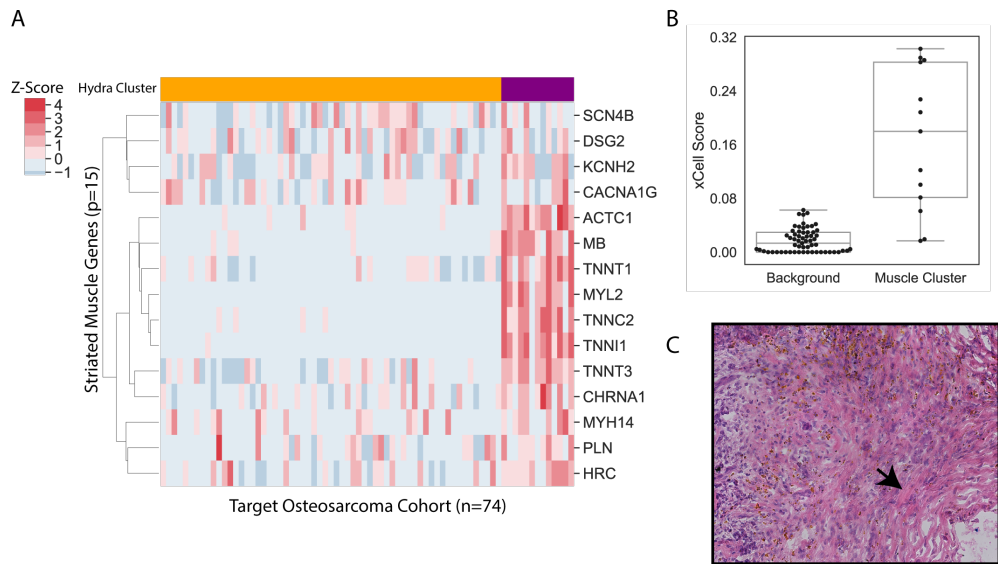


Fig 5. Hydra analysis of TARGET osteosarcoma cohort reveals skeletal muscle signature. Hydra enrichment analysis on the TARGET osteosarcoma cohort revealed a subset of patients with high skeletal muscle expression. A: Clustered heatmap shows the muscle signature genes identified by hydra unsupervised enrichment analysis (purple: enriched for muscle signature; yellow: not enriched for muscle signature). B: xCell tumor microenvironment profiling identified significant differences in skeletal muscle expression compared to background ($p < 0.001$). C: H&E stained tumor slide confirms presence of striated muscle tissue within the tumor sample.

(Kruskal-Wallis test: Holm-Sidak adjusted p -value < 0.05 , S1 File). Some of the druggable genes were expected to correlate with non-cancer cells, including the cytokines *IL6* and *TGFB2*, which correlated with epithelial cells and fibroblasts, respectively. Other druggable genes were surprising, like *AURKA* and *AURKB*, which correlated with higher Th2 cell expression. Aurora kinases play essential roles in spindle formation during mitosis and the overexpression of these genes is associated with evading spindle formation checkpoints in cancer [68], but little is known in how these genes correlate with infiltrating immune cells. Aurora kinase inhibitors show limited clinical activity in solid tumors, but have been shown to have a greater effect in leukemias [68, 69].

Hydra analysis reveals recurrent expression subtypes across small blue round cell tumors

We next investigated whether similar hydra clusters could be identified across other small blue round cell tumors. We chose to focus on extracranial solid tumors because they are among the most common pediatric cancers, making up 20% of all pediatric cancer diagnoses [70], and while survival rates have improved, there are few effective treatment options for the subset of patients with relapse or refractory disease [71]. Identifying expression subtypes for these diseases may improve risk stratification and discover opportunities for new therapies. These tumors also share similar histopathological features, so we hypothesized that these tumors may share similar gene expression subtypes, despite significant differences in the raw expression profiles (Fig 6A).

We first performed TumorMap analysis, which is a dimensionality reduction approach for visualizing genomic data on a 2D surface [5]. We found that small blue

round cell tumor types — *MYCN*-NA neuroblastoma, osteosarcoma, Ewing sarcoma, synovial sarcoma, alveolar rhabdomyosarcoma, and embryonal rhabdomyosarcoma — all form separate TumorMap clusters (Fig 6A). This suggests there is a strong cell-of-origin signal driving the clustering of these cancer types, which is an observation that was recently made in the larger TCGA dataset of adult cancers [72]. While pan-cancer analysis emphasized the differences across small blue round cell tumors, we hypothesized that expression subtypes within cancer types would participate in shared biological themes.

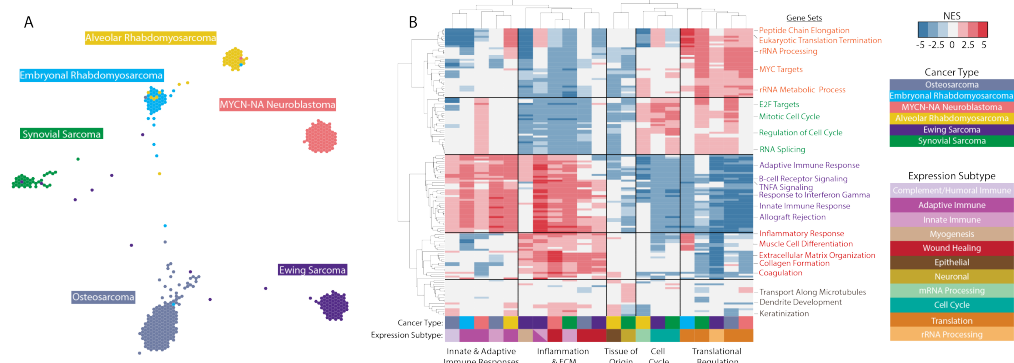


Fig 6. Hydra *enrich* analysis of small blue round cell tumors reveals similar expression subtypes across cancer types. A: TumorMap visualization of 6 small blue round cell tumor types. B: Hierarchically clustered heatmap for the top 10 enriched gene sets across the 21 small blue round cell tumor expression subtypes. Each column corresponds to a cancer type and an expression subtype (x-axis). Each row corresponds to a gene set. The expression subtype was manually assigned after reviewing the most highly enriched gene sets for each cancer expression subtype.

We next performed hydra *enrich* analysis within each small round blue cell cancer type and found shared biological themes across all six small blue round tumor types. Hierarchical clustering of the top 10 statistically significant gene sets for each cancer type resulted in clustering by expression subtype and not the cancer type (Fig 6B). Common themes emerged across diseases including translational regulation, cell cycle regulation, immune effector cell signaling, inflammation, extracellular matrix organization, and tissue-of-origin signals. Furthermore, these signals predicted differences in patient outcomes in osteosarcoma and synovial sarcoma (Fig 7). In both cases, the presence of immune-associated expression correlated with better patient outcomes compared to tumors with proliferative signaling pathways associated with translation initiation and cell cycle regulation. Other osteosarcoma clusters were not included in the survival analysis due to insufficient number of samples with survival data ($n < 5$). Survival data were not available for the rhabdomyosarcoma and Ewing sarcoma expression datasets.

Discussion

The hydra framework uses model-based clustering to facilitate the discovery of recurrent expression patterns within cancer gene expression cohorts. We leveraged recent improvements in model-based clustering algorithms to identify differentially expressed genes without a matched normal distribution. We modeled differential expression as a multimodal Gaussian distribution using nonparametric Bayesian statistics. We then enriched for biologically-annotated Gene Ontology terms and performed multivariate

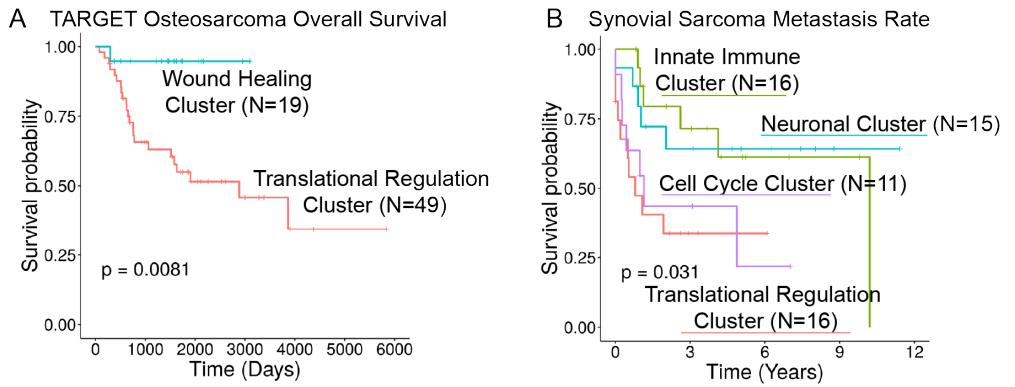


Fig 7. Hydra analysis identifies tumor microenvironment expression subtypes that correlate with patient outcomes in osteosarcoma and synovial sarcoma. A: Kaplan-Meier plot showing overall survival curves for osteosarcoma wound healing and translation clusters. B: Kaplan-Meier plot showing metastasis survival curves for synovial sarcoma clusters.

clustering to reveal expression subtypes. The hydra framework can be used for both identifying expression subtypes within large cohorts and classifying new tumor gene expression profiles using the trained models. The hydra framework outperformed standard gene set enrichment tools for identifying overexpression of the MSigDB Hallmark cancer gene sets in synthetic data. Application of this framework to small blue round cell tumors identified shared biological themes associated with the tumor microenvironment.

Multivariate gene expression analysis is typically underpowered because the number of genes greatly exceeds the number of samples. To address this limitation, we propose selecting for multimodally expressed genes before performing multivariate analysis. The hydra *filter* method reduces the number of genes and enriches for genes that participate in known biological processes, including those curated in the Gene Ontology and MSigDB databases. Selecting for multimodally expressed genes improves separation of known clinical subtypes better than the standard approach of using all expressed genes according to TumorMap analysis (S2 Fig). We also showed that the hydra approach of subsetting to multimodal genes improves detection of differential pathway expression, including the identification of expression subtypes associated with the TME.

Significant progress has been made in subtyping neuroblastomas and adapting therapy for aggressive subtypes, but unexplained heterogeneity remains [59]. Failure to account for this heterogeneity decreases the power of standard methods to detect important expression patterns. Identifying biomarkers using genome-wide technology may lead to improved risk stratification and the discovery of novel drug targets. Hydra analysis of the TARGET *MYCN*-NA neuroblastoma cohort found differential expression of tumor microenvironment markers, including markers of the adaptive immune response. Pediatric cancers are generally thought to be less immunogenic because they have lower mutation burdens than adult cancers, but the immunogenicity of pediatric cancer has not been sufficiently investigated [11, 12].

Our analysis found significant variation in immune marker expression, including markers of response to checkpoint blockade therapy, and identified *ATRX* deletions as a potential biomarker of immune infiltrated tumors in *MYCN*-NA neuroblastoma. Analysis of other small blue round cell tumors revealed similar expression signatures across tumor types, despite samples clustering by their histology in a pan-cancer TumorMap analysis. Identification of shared expression signatures across cancer types

may suggest that these patients would respond similarly to therapies that target these pathways. In particular, the identification of a cross-disease subtype associated with high expression of immune markers may warrant further investigation of immunotherapies in small blue round cell tumors using a basket clinical trial design [73].

Hydra analysis found significant differences in tumor immune and stromal expression that may inform precision medicine applications. The tumor microenvironment has become an important therapeutic consideration, but few methods account for the tumor microenvironment directly. Tumor purity has been identified as a confounding factor in cancer gene expression subtyping efforts [74]. For example, tumor purity and tumor microenvironment expression have been shown to correlate with pancreatic cancer subtypes [75]. Furthermore, Aran et al. (2018) found that tumor purity was correlated with the mesenchymal glioblastoma subtype and recommended a differential expression approach to computationally remove the tumor purity signal. However, standard approaches for subtracting the tumor purity effect may not be ideal because several mechanisms may influence tumor purity, and each mechanism may result in a different expression pattern. For instance, our analysis of *MYCN*-NA neuroblastoma identified two gene expression signatures that correlated with lower predicted tumor purity. Cluster 1 had an adaptive immune expression signature and cluster 3 had a cancer-associated fibroblast signature. Therefore, the estimated tumor purity signal should not be subtracted without first accounting for the different mechanisms influencing tumor purity.

We also found shared biological pathway enrichment across small blue round cell tumors. While these diseases are related and may derive from similar cell lineages, current expression methods often emphasize difference across these diseases (Fig 6A). Unsupervised clustering of adult cancer types found that cell-of-origin signals strongly influence clustering of cancer gene expression data [72]. Although these diseases have distinct expression patterns on the surface, we discovered common themes once we subset the data to the cell-of-origin signal and applied the hydra analysis tools.

We found at least three shared TME states: immune silent, immune infiltrated, and wound healing subtypes. The wound healing subtypes predicted better overall survival in osteosarcoma and delayed metastases in synovial sarcoma tumors, which suggests the involvement of the host immune response limits the progression of these tumors. Amplification of the host immune response may further limit tumor growth and lead to immune-mediated tumor cell death. Additional research into immune modulating therapies is warranted in small blue round cell tumors and may lead to improved outcomes for some patients.

Conclusion

Precision oncology aims to differentiate tumors of the same diagnosis in order to match patients with the best treatment. We have developed the hydra framework to discover subtle but recurrent expression patterns within a cohort of samples with the same diagnosis, which is a novel strategy for pediatric precision oncology research. Our approach may help to uncover the biology underlying tumor progression and response to therapy. We have shown that hydra is more sensitive than standard gene set enrichment approaches for detecting differential pathway expression. Additionally, our framework provides tools to conduct unsupervised clustering analysis to discover expression subtypes. We applied the unsupervised hydra analysis to small blue round cell tumors and discovered distinct tumor microenvironment (TME) states. This shows that one of the strongest signals in clinical gene expression data comes from the TME, so careful modeling of the TME is required to maximize the impact of clinical gene expression analysis. The hydra framework provides unbiased clustering tools to characterize these

sources of variation in specific disease populations and identify shared biological themes
that can potentially be targeted therapeutically.

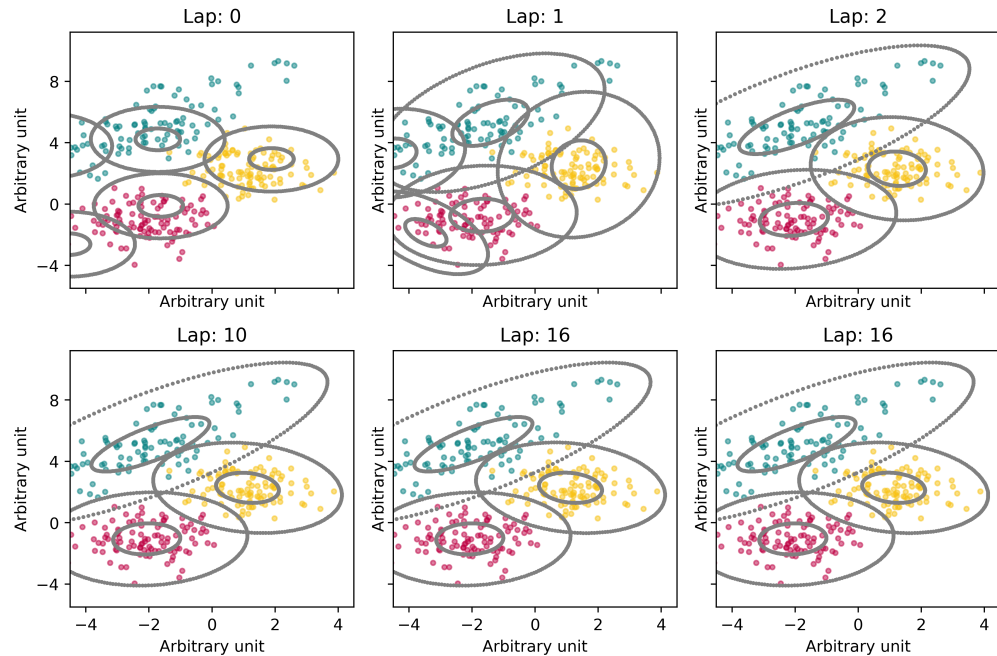
659
660

Supporting information

661

S1 Fig.

662

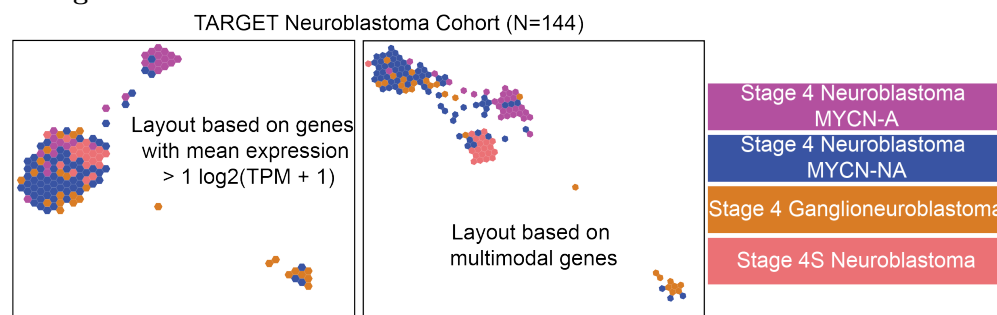


663
664
665
666
667
668

Example of bnpv memoized online variational inference clustering on toy data. We used the bnpv moVB algorithm to infer the number of clusters from synthetic data. The model first randomly assigns clusters. Then, the model iteratively improves the model fit, creating and destroying clusters until the model converges on the correct number of clusters at lap 16 [36].

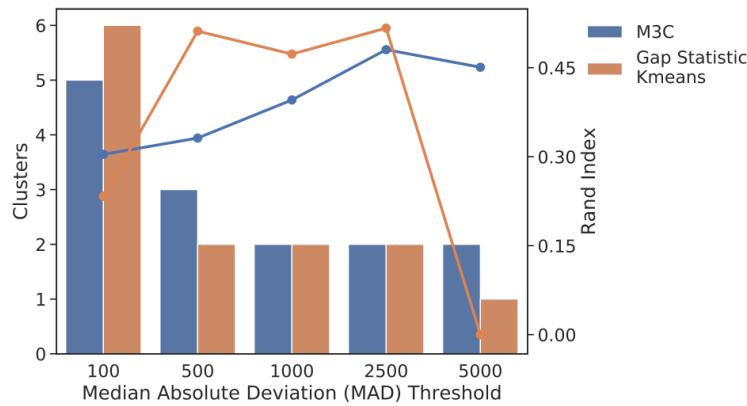
S2 Fig.

669



670
671
672
673
674
675
676

Enriching for multimodally expressed genes improves clustering of established neuroblastoma subtypes. Standard TumorMap analysis of the TARGET neuroblastoma dataset resulted in stage 4S samples clustering with stage 4 neuroblastoma samples (left). An alternative TumorMap based solely on 1,498 multimodally expressed genes separated the stage 4S samples into a distinct cluster (right).

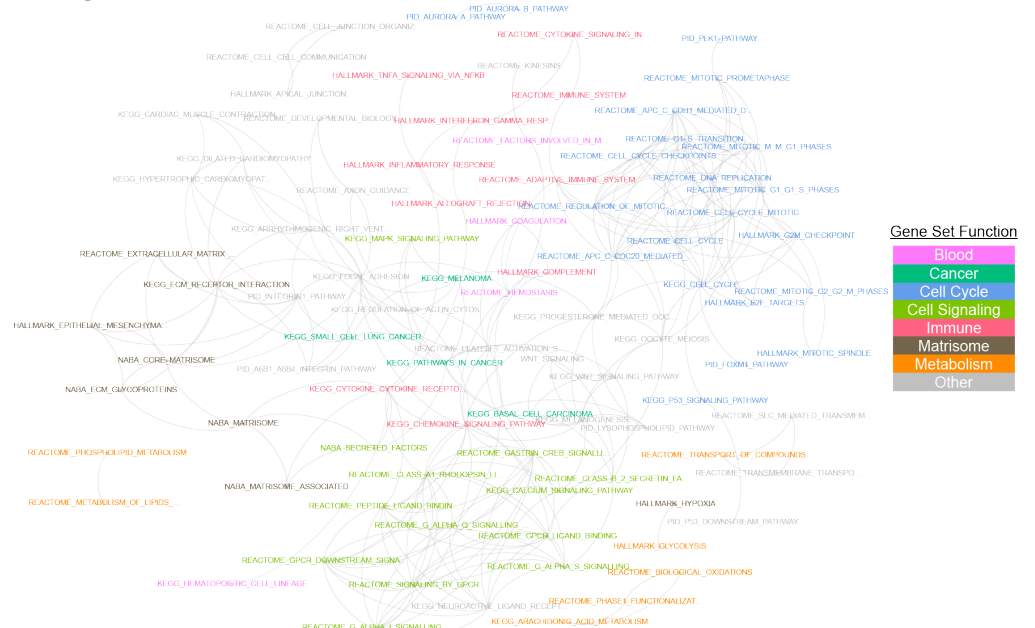


S3 Fig.

Consensus and k-means clustering applied to TARGET MYCN-NA dataset.

We tested a range of gene expression variation thresholds based on the median absolute deviation, but found that the clusters identified by this approach could not resolve the same clusters as the hydra approach. The barplot shows the number of clusters and the lineplot tracks the Rand index comparing the M3C and k-means clusters and the hydra clusters.

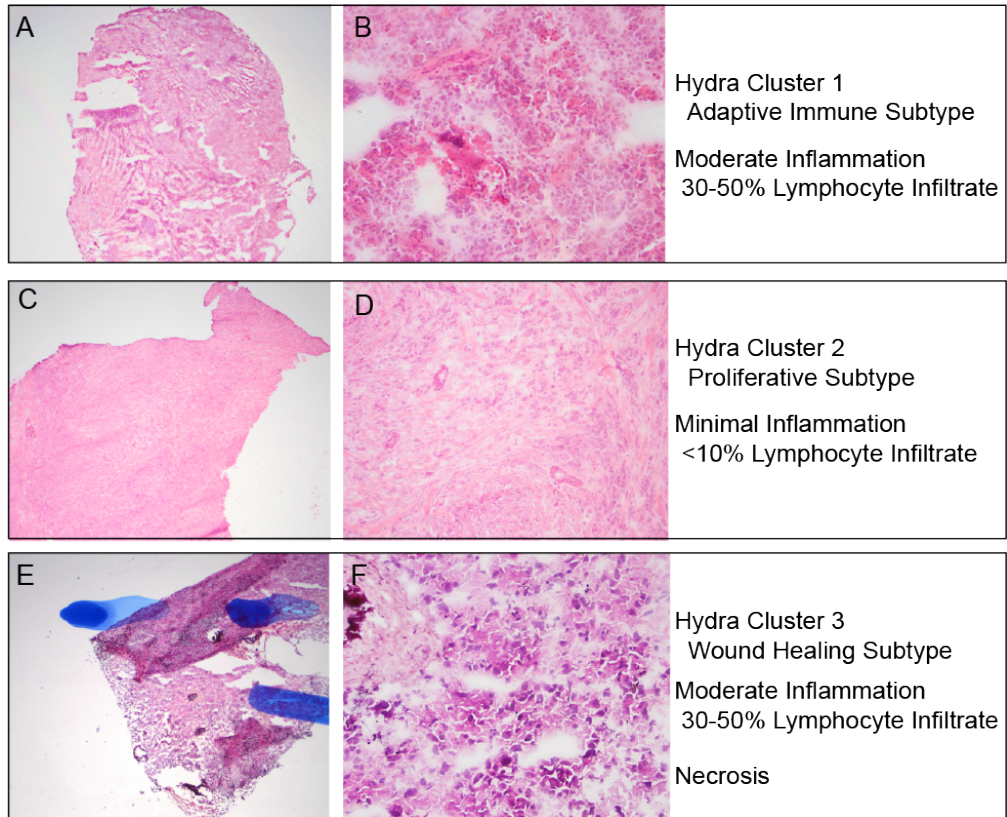
S4 Fig.



Hydra sweep analysis reveals differential pathway expression within MYCN-NA neuroblastoma without a matched cohort of normal tissue.

Unsupervised clustering of multimodal gene sets revealed biological themes associated with hallmark cancer functions, including cell cycle, immune cell signaling, extracellular matrix organization, and metabolism.

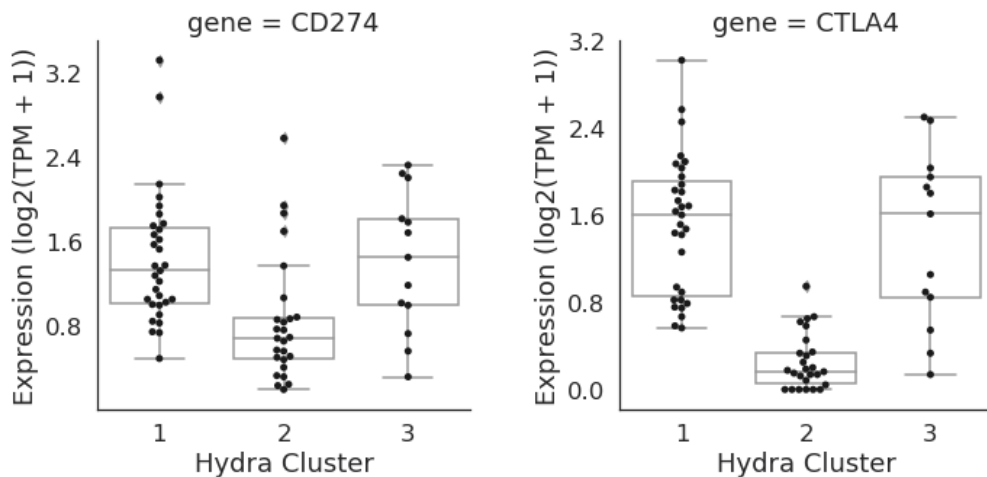
S5 Fig.



Hydra method correlates with distinct tumor features as assessed by licensed pathologist review of tumor H&E slides. A-B: H&E sections from fresh frozen tumor tissue from *MYCN*-NA neuroblastoma sample at A: 2X magnification and B: 20X magnification. Tumor cells are medium to large with moderate amounts of cytoplasm and areas of rhabdoid appearing undifferentiated cells. There is a moderate amount of mixed inflammation present (30-50%) consisting mostly of mature mononuclear cells with some plasma cells and scattered eosinophils. C-D: H&E sections from fresh frozen tumor tissue from *MYCN*-NA neuroblastoma at C: 2X magnification and D: 20X magnification. Tumor cells are moderate to large in size with moderate amounts of cytoplasm. There is a minimal amount (<10%) of apparent mononuclear inflammation scattered throughout the tumor. E-F: H&E sections from fresh frozen tumor tissue from *MYCN*-NA neuroblastoma sample at (E) 2X magnification and (F) 20X magnification. Tumor cells are medium to large with moderate amounts of cytoplasm and areas of rhabdoid appearing undifferentiated cells. There are also areas of apparent necrosis. There is a moderate amount of inflammation present (30-50%) consisting mostly of mature mononuclear cells with some plasma cells and scattered eosinophils.

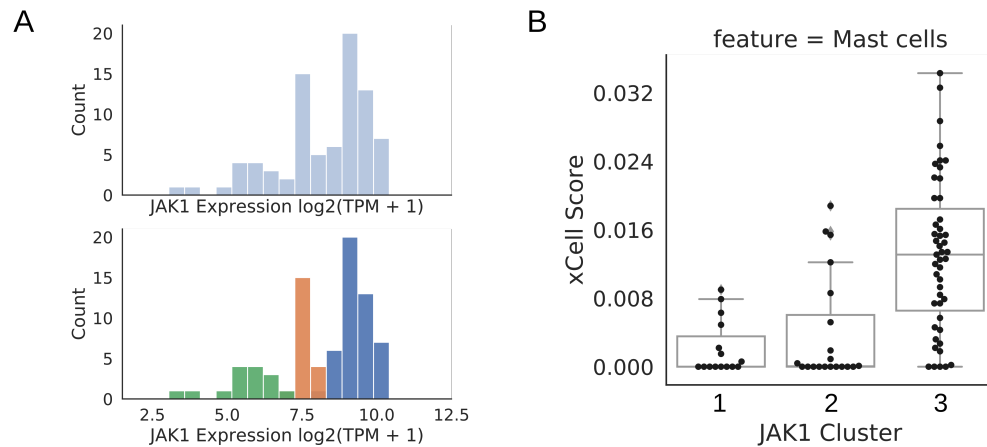
692
693
694
695
696
697
698
699
700
701
702
703
704
705
706
707
708
709

S6 Fig.



Hydra *enrich* analysis identifies correlation between expression subtypes and checkpoint blockade markers in *MYCN*-NA neuroblastoma. 710
711
712
713

S7 Fig.



Hydra analysis identified *JAK1* expression clusters that correlate with mast cell expression signature in Ewing sarcoma. A: *JAK1* expression distribution for Ewing sarcoma cohort (top) and the *JAK1* expression distributions for cluster 1 (green), 2 (orange), and 3 (blue). B: Boxplot showing the xCell mast cell enrichment score for the three clusters associated with *JAK1* expression. 714
715
716
717
718
719
720

S1 File. TARGET *MYCN*-NA neuroblastoma supplementary data. 721

S2 File. Hydra method documentation. 722

Acknowledgments

We would like to thank the patients and families who participated in translational genomics research. We would also like to thank the St. Baldrick's Foundation, the California Initiative to Advance Precision Medicine, and the National Human Genome Research Institute of the National Institutes of Health for funding support. 723
724
725
726
727

References

1. Vivian J, Rao AA, Nothaft FA, Ketchum C, Armstrong J, Novak A, et al. Toil Enables Reproducible, Open Source, Big Biomedical Data Analyses;35(4):314–316. doi:10.1038/nbt.3772.
2. Pugh TJ, Morozova O, Attiyeh EF, Asgharzadeh S, Wei JS, Auclair D, et al. The Genetic Landscape of High-Risk Neuroblastoma;45(3):279–284. doi:10.1038/ng.2529.
3. Goldman M, Craft B, Kamath A, Brooks A, Zhu J, Haussler D. The UCSC Xena Platform for Cancer Genomics Data Visualization and Interpretation; p. 326470. doi:10.1101/326470.
4. The Cancer Genome Atlas Research Network, Weinstein JN, Collisson EA, Mills GB, Shaw KRM, Ozenberger BA, et al. The Cancer Genome Atlas Pan-Cancer Analysis Project;45:1113–1120. doi:10.1038/ng.2764.
5. Newton Y, Novak AM, Swatloski T, McColl DC, Chopra S, Graim K, et al. TumorMap: Exploring the Molecular Similarities of Cancer Samples in an Interactive Portal;77(21):e111–e114. doi:10.1158/0008-5472.CAN-17-0580.
6. Vaske OM, Bjork I, Salama SR, Beale H, Shah AT, Sanders L, et al. Comparative Tumor RNA Sequencing Analysis for Difficult-to-Treat Pediatric and Young Adult Patients With Cancer;2(10):e1913968–e1913968. doi:10.1001/jamanetworkopen.2019.13968.
7. Joyce JA, Fearon DT. T Cell Exclusion, Immune Privilege, and the Tumor Microenvironment;348(6230):74–80. doi:10.1126/science.aaa6204.
8. Chen DS, Mellman I. Elements of Cancer Immunity and the Cancer–Immune Set Point;541(7637):321–330. doi:10.1038/nature21349.
9. Mellman I, Coukos G, Dranoff G. Cancer Immunotherapy Comes of Age;480(7378):480–489. doi:10.1038/nature10673.
10. Page DB, Postow MA, Callahan MK, Allison JP, Wolchok JD. Immune Modulation in Cancer with Antibodies;65:185–202. doi:10.1146/annurev-med-092012-112807.
11. Majzner RG, Heitzeneder S, Mackall CL. Harnessing the Immunotherapy Revolution for the Treatment of Childhood Cancers;31(4):476–485.
12. Zamora AE, Crawford JC, Allen EK, Guo XzJ, Bakke J, Carter RA, et al. Pediatric Patients with Acute Lymphoblastic Leukemia Generate Abundant and Functional Neoantigen-Specific CD8+ T Cell Responses;11(498). doi:10.1126/scitranslmed.aat8549.
13. Anders S, McCarthy DJ, Chen Y, Okoniewski M, Smyth GK, Huber W, et al. Count-Based Differential Expression Analysis of RNA Sequencing Data Using R and Bioconductor;8(9):1765–1786. doi:10.1038/nprot.2013.099.
14. Anders S, Huber W. Differential Expression Analysis for Sequence Count Data;11(10):R106. doi:10.1186/gb-2010-11-10-r106.
15. Soneson C, Delorenzi M. A Comparison of Methods for Differential Expression Analysis of RNA-Seq Data;14(1):91. doi:10.1186/1471-2105-14-91.

16. Subramanian A, Tamayo P, Mootha VK, Mukherjee S, Ebert BL, Gillette MA, et al. Gene Set Enrichment Analysis: A Knowledge-Based Approach for Interpreting Genome-Wide Expression Profiles;102(43):15545–15550. doi:10.1073/pnas.0506580102.
17. Mootha VK, Lindgren CM, Eriksson KF, Subramanian A, Sihag S, Lehar J, et al. PGC-1alpha-Responsive Genes Involved in Oxidative Phosphorylation Are Coordinately Downregulated in Human Diabetes;34(3):267–273. doi:10.1038/ng1180.
18. Liberzon A, Subramanian A, Pinchback R, Thorvaldsdóttir H, Tamayo P, Mesirov JP. Molecular Signatures Database (MSigDB) 3.0;27(12):1739–1740. doi:10.1093/bioinformatics/btr260.
19. Oyelade J, Isewon I, Oladipupo F, Aromolaran O, Uwoghiren E, Ameh F, et al. Clustering Algorithms: Their Application to Gene Expression Data;10:237–253. doi:10.4137/BBI.S38316.
20. John CR, Watson D, Russ D, Goldmann K, Ehrenstein M, Lewis M, et al. M3C: A Monte Carlo Reference-Based Consensus Clustering Algorithm; p. 377002.
21. Wilkerson MD, Hayes DN. ConsensusClusterPlus: A Class Discovery Tool with Confidence Assessments and Item Tracking;26(12):1572–1573. doi:10.1093/bioinformatics/btq170.
22. Lenz M, Müller FJ, Zenke M, Schuppert A. Principal Components Analysis and the Reported Low Intrinsic Dimensionality of Gene Expression Microarray Data;6(1):1–11. doi:10.1038/srep25696.
23. Ghosh D. Mixture Models for Assessing Differential Expression in Complex Tissues Using Microarray Data;20(11):1663–1669. doi:10.1093/bioinformatics/bth139.
24. Dahl DB, Vannucci M. In: Do KA, Muller P, editors. Model-Based Clustering for Expression Data via a Dirichlet Process Mixture Model. Cambridge University Press; p. 201–218. Available from: https://www.cambridge.org/core/product/identifier/CB09780511584589A070/type/book_part.
25. Kim S, Tadesse MG, Vannucci M. Variable Selection in Clustering via Dirichlet Process Mixture Models;93(4):877–893. doi:10.1093/biomet/93.4.877.
26. Gelman A, Carlin JB, Stern HS, Dunson DB, Vehtari A, Rubin DB, et al. Bayesian Data Analysis. Chapman and Hall/CRC;. Available from: <https://www.taylorfrancis.com/books/9780429113079>.
27. Thall PF, Mueller P, Xu Y, Guindani M. Bayesian Nonparametric Statistics: A New Toolkit for Discovery in Cancer Research;16(6):414–423. doi:10.1002/pst.1819.
28. Teh YW. Dirichlet Process; p. 280–287.
29. Antoniak CE. Mixtures of Dirichlet Processes with Applications to Bayesian Nonparametric Problems;2(6):1152–1174. doi:10.1214/aos/1176342871.
30. Ferguson TS. A Bayesian Analysis of Some Nonparametric Problems;1(2):209–230. doi:10.1214/aos/1176342360.
31. Müller P, Quintana FA. Nonparametric Bayesian Data Analysis; p. 95–110.

32. Görür D, Edward Rasmussen C. Dirichlet Process Gaussian Mixture Models: Choice of the Base Distribution;25(4):653–664. doi:10.1007/s11390-010-9355-8.
33. Hughes MC, Sudderth E. Memoized Online Variational Inference for Dirichlet Process Mixture Models. In: Advances in Neural Information Processing Systems;,. p. 1133–1141.
34. Müller P, Quintana FA, Jara A, Hanson T. Bayesian Nonparametric Data Analysis. Springer Series in Statistics. Springer International Publishing; Available from: <https://www.springer.com/gp/book/9783319189673>.
35. Phadia EG. Prior Processes and Their Applications. Springer;.
36. Hughes MC, Sudderth EB. Bnpy : Reliable and Scalable Variational Inference for Bayesian Nonparametric Models; p. 4.
37. Ashburner M, Ball CA, Blake JA, Botstein D, Butler H, Cherry JM, et al. Gene Ontology: Tool for the Unification of Biology;25(1):25–29. doi:10.1038/75556.
38. Consortium GO. The Gene Ontology Resource: 20 Years and Still GOing Strong;47(D1):D330–D338.
39. Merico D, Isserlin R, Stueker O, Emili A, Bader GD. Enrichment Map: A Network-Based Method for Gene-Set Enrichment Visualization and Interpretation;5(11):e13984.
40. Yu G, Wang LG, Han Y, He QY. clusterProfiler: An R Package for Comparing Biological Themes among Gene Clusters;16(5):284–287. doi:10.1089/omi.2011.0118.
41. Cai T, Liu W, Luo X. A Constrained ℓ_1 Minimization Approach to Sparse Precision Matrix Estimation;106(494):594–607. doi:10.1198/jasa.2011.tm10155.
42. Tamayo P, Steinhardt G, Liberzon A, Mesirov JP. The Limitations of Simple Gene Set Enrichment Analysis Assuming Gene Independence;25(1):472–487. doi:10.1177/0962280212460441.
43. Korotkevich G, Sukhov V, Sergushichev A. Fast Gene Set Enrichment Analysis; p. 060012. doi:10.1101/060012.
44. Barbie DA, Tamayo P, Boehm JS, Kim SY, Moody SE, Dunn IF, et al. Systematic RNA Interference Reveals That Oncogenic KRAS-Driven Cancers Require TBK1;462(7269):108–112. doi:10.1038/nature08460.
45. Hänelmann S, Castelo R, Guinney J. GSVA: Gene Set Variation Analysis for Microarray and RNA-Seq Data;14(1):7. doi:10.1186/1471-2105-14-7.
46. Tarca AL, Bhatti G, Romero R. A Comparison of Gene Set Analysis Methods in Terms of Sensitivity, Prioritization and Specificity;8(11):e79217. doi:10.1371/journal.pone.0079217.
47. Zwiener I, Frisch B, Binder H. Transforming RNA-Seq Data to Improve the Performance of Prognostic Gene Signatures;9(1):e85150. doi:10.1371/journal.pone.0085150.
48. Lagarde P, Przybyl J, Brulard C, Pérot G, Pierron G, Delattre O, et al. Chromosome Instability Accounts for Reverse Metastatic Outcomes of Pediatric and Adult Synovial Sarcomas;31(5):608–615. doi:10.1200/JCO.2012.46.0147.

49. Bastian M, Heymann S, Jacomy M. Gephi: An Open Source Software for Exploring and Manipulating Networks. In: Third International AAAI Conference on Weblogs and Social Media;.
50. Aran D, Hu Z, Butte AJ. xCell: Digitally Portraying the Tissue Cellular Heterogeneity Landscape;18(1):220. doi:10.1186/s13059-017-1349-1.
51. Newman AM, Liu CL, Green MR, Gentles AJ, Feng W, Xu Y, et al. Robust Enumeration of Cell Subsets from Tissue Expression Profiles;12(5):453–457. doi:10.1038/nmeth.3337.
52. Yoshihara K, Shahmoradgoli M, Martínez E, Vegesna R, Kim H, Torres-Garcia W, et al. Inferring Tumour Purity and Stromal and Immune Cell Admixture from Expression Data;4:2612. doi:10.1038/ncomms3612.
53. Tibshirani R, Walther G, Hastie T. Estimating the Number of Clusters in a Data Set via the Gap Statistic;63(2):411–423.
54. Pedregosa F, Varoquaux G, Gramfort A, Michel V, Thirion B, Grisel O, et al. Scikit-Learn: Machine Learning in Python;12:2825–2830.
55. Jones E, Oliphant T, Peterson P, et al. SciPy: Open Source Scientific Tools for Python;.
56. Virtanen P, Gommers R, Oliphant TE, Haberland M, Reddy T, Cournapeau D, et al. SciPy 1.0—Fundamental Algorithms for Scientific Computing in Python; p. arXiv:1907.10121.
57. Terpilowski M. Scikit-Posthocs: Pairwise Multiple Comparison Tests in Python;4(36):1169. doi:10.21105/joss.01169.
58. Kassambara A, Kosinski M, Biecek P. Survminer: Drawing Survival Curves Using 'Ggplot2';. Available from: <https://CRAN.R-project.org/package=survminer>.
59. Morgenstern DA, Bagatell R, Cohn SL, Hogarty MD, Maris JM, Moreno L, et al. The Challenge of Defining “Ultra-High-Risk” Neuroblastoma;66(4):e27556. doi:10.1002/pbc.27556.
60. Cotto KC, Wagner AH, Feng YY, Kiwala S, Coffman AC, Spies G, et al. DGIdb 3.0: A Redesign and Expansion of the Drug–Gene Interaction Database;46(D1):D1068–D1073.
61. Foster DS, Jones RE, Ransom RC, Longaker MT, Norton JA. The Evolving Relationship of Wound Healing and Tumor Stroma;3(18). doi:10.1172/jci.insight.99911.
62. Bourgon R, Gentleman R, Huber W. Independent Filtering Increases Detection Power for High-Throughput Experiments;107(21):9546–9551. doi:10.1073/pnas.0914005107.
63. Tritchler D, Parkhomenko E, Beyene J. Filtering Genes for Cluster and Network Analysis;10(1):193. doi:10.1186/1471-2105-10-193.
64. Carcamo-Orive I, Hoffman GE, Cundiff P, Beckmann ND, D’Souza SL, Knowles JW, et al. Analysis of Transcriptional Variability in a Large Human iPSC Library Reveals Genetic and Non-Genetic Determinants of Heterogeneity;20(4):518–532.e9. doi:10.1016/j.stem.2016.11.005.

65. Maechler M, Rousseeuw P, Struyf A, Hubert M, Hornik K, et al. Cluster: Cluster Analysis Basics and Extensions;1(2):56.
66. Reeves E, James E. Antigen Processing and Immune Regulation in the Response to Tumours;150(1):16–24. doi:10.1111/imm.12675.
67. Hermans MAW, Schrijver B, van Holten-Neelen CCPA, Gerth van Wijk R, van Hagen PM, van Daele PLA, et al. The JAK1/JAK2- Inhibitor Ruxolitinib Inhibits Mast Cell Degranulation and Cytokine Release;48(11):1412–1420. doi:10.1111/cea.13217.
68. Maris JM, Morton CL, Gorlick R, Kolb EA, Lock R, Carol H, et al. Initial Testing of the Aurora Kinase a Inhibitor MLN8237 by the Pediatric Preclinical Testing Program (PPTP);55(1):26–34. doi:10.1002/pbc.22430.
69. Gautschi O, Heighway J, Mack PC, Purnell PR, Lara PN, Gandara DR. Aurora Kinases as Anticancer Drug Targets;14(6):1639–1648. doi:10.1158/1078-0432.CCR-07-2179.
70. Ries LaG, Smith MA, Gurney JG, Linet M, Tamra T, Young JL, et al. Cancer Incidence and Survival among Children and Adolescents: United States SEER Program 1975-1995.;.
71. Ring EK, Markert JM, Gillespie GY, Friedman GK. Checkpoint Proteins in Pediatric Brain and Extracranial Solid Tumors: Opportunities for Immunotherapy;23(2):342–350. doi:10.1158/1078-0432.CCR-16-1829.
72. Hoadley KA, Yau C, Hinoue T, Wolf DM, Lazar AJ, Drill E, et al. Cell-of-Origin Patterns Dominate the Molecular Classification of 10,000 Tumors from 33 Types of Cancer;173(2):291–304.e6. doi:10.1016/j.cell.2018.03.022.
73. Cunanan KM, Iasonos A, Shen R, Begg CB, Gönen M. An Efficient Basket Trial Design;36(10):1568–1579. doi:10.1002/sim.7227.
74. Rhee JK, Jung YC, Kim KR, Yoo J, Kim J, Lee YJ, et al. Impact of Tumor Purity on Immune Gene Expression and Clustering Analyses across Multiple Cancer Types;6(1):87–97. doi:10.1158/2326-6066.CIR-17-0201.
75. Raphael BJ, Hruban RH, Aguirre AJ, Moffitt RA, Yeh JJ, Stewart C, et al. Integrated Genomic Characterization of Pancreatic Ductal Adenocarcinoma;32(2):185–203.